

PAPER • OPEN ACCESS

Tribological and corrosion behavior of HVAF-sprayed (Fe-TiB₂)/CNT composite coating

To cite this article: Xiaoqing Liu *et al* 2021 *J. Phys.: Conf. Ser.* **2044** 012005

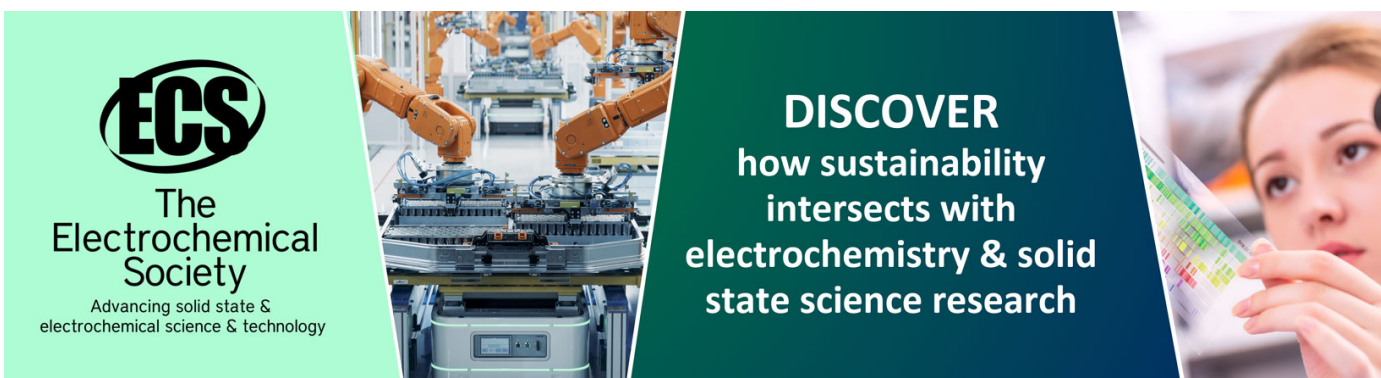
View the [article online](#) for updates and enhancements.

You may also like

- [Design and implementation of active frequency control algorithm for virtual power plant based on flexible resource rapid response](#)
Bin Li and Junjie Yu

- [Interaction of DNA/nuclear protein/polycation and the terplexes for gene delivery](#)
Yuan Shen, Hui Peng, Shirong Pan et al.

- [Effects of process parameters on morphologies of titanium carbide powder by thermal plasma treatment](#)
Sihui Zeng, Meng Xiao, Xiaoqing Liu et al.



ECS
The
Electrochemical
Society
Advancing solid state &
electrochemical science & technology

DISCOVER
how sustainability
intersects with
electrochemistry & solid
state science research

Tribological and corrosion behavior of HVAF-sprayed (Fe-TiB₂)/CNT composite coating

Xiaoqing Liu ^{1,2,a}, Yaosha Wu ^{3,b}, Shiye Zhuo ^{1,2,c}, Zhengyi Lu ^{4,d}, Shunqiang Yao ^{4,e}, Zhaoguo Qiu ^{1,2,f}, Dechang Zeng ^{1,2,g*}

¹ School of Materials Science and Engineering, South China University of Technology, Guangzhou 510640, China

² Zhongshan R&D Center for Materials Surface and Thin Films Technology of the South China University of Technology, Gent Materials Surface Technology (Guangdong) Co., Ltd, Zhongshan 528437, China

³ Zhongshan Torch Polytechnic, Zhongshan 528436, China

⁴ Zhongshan Zhongsheng Metallic Plate and Strip Science and Technology Co., Ltd, Zhongshan 528441, China

^aemail: 201811004664@mail.scut.edu.cn, ^bemail: 547656588@qq.com, ^cemail: 363605788@qq.com, ^demail: luzhengyi@vip.sina.com, ^eemail: 13711739171@139.com, ^femail: zgqiu@scut.edu.cn

*Corresponding author: ^gemail: medczeng@scut.edu.cn

Abstract: Fe-based composite coating doped well-dispersed titanium boride (TiB₂) and carbon nanotubes (CNTs) was fabricated via combined ball milling, spray drying, plasma spheroidization and high velocity air fuel (HVAF) spraying. The microstructure evolution of composite powders and coating, the tribological and corrosion behavior of Fe-based metallic, Fe-TiB₂ cermet and (Fe-TiB₂)/CNT composite coatings were investigated. The results show that doping 50 vol. % TiB₂, especially further doping 2.5 vol. % CNTs could remarkably render the coating favorable microstructure with low porosity, enhanced hardness and fracture toughness, and superior wear and corrosion resistance. Mild oxidative and slight abrasive wears were the dominant wear mechanism, and the preferential corrosion was occurred at the pores, inter-splats and then the TiB₂-Fe interfaces.

1. Introduction

Wear and corrosion are two common kinds of failure modes for the mechanical components. To prolong the service life of workpieces, thermal sprayed protective coatings to their surface have been proved to be effective. Among the coatings, Fe-based coatings recently have been intensively investigated for its distinct advantages of low harm and cost [1, 2]. It is noted that quite a few Fe-based coatings as alternatives have shown their prospects in wear and corrosion properties [3]. However, to meet the ever-increasing demands of modern industry, numerous techniques have been tried to fabricate high performance Fe-based coatings. So far, quite a few attempts such as optimizing the spray parameters [4, 5], powder size [6, 7] and spray methods [8], doping second phase [9-11] or achieving nanostructured microstructure [12, 13] were proposed to enhance the wear and corrosion resistance of coatings.



Among them, introduction of second phase into the coating is regarded as a more efficient method due to the synergistic effects of reinforcements. In term of the Fe-based metallic coating, it needs to add high hardness second phase to improve its resistance to aggressive environments. Both the titanium diboride (TiB_2) and carbon nanotube (CNT) were well-known for their super high hardness or strength, which shows great potential as reinforcements to fabricate composite materials [14, 15]. However, to better achieve their strengthening effect, the preparation of feedstock for spraying is very crucial. Until now, rare researches have tried to simultaneously dope TiB_2 and CNTs into the Fe-based coating, and its strengthening mechanism also needs to be further clarified.

Thus, in this work, Fe-based coating doped with TiB_2 and CNTs was deposited via high velocity air fuel (HVOF) spraying. And the effects of the TiB_2 and CNTs on the microstructure and tribological and corrosion properties were investigated. In addition, the underlying mechanisms were also discussed.

2. Materials and methods

2.1 Coatings fabrication

Fe60A self-fluxing alloy powders with a size range from 17 to 49 μm , highly purified TiB_2 powders with a size range from 3 to 13 μm and graphitized multi-walled CNTs with a diameter of 10-20 nm and length of 5-30 μm were employed as starting materials. Firstly, ball milling was utilized to get the composite mixture with homogeneous CNTs and TiB_2 particles. In detail, 50 vol. % TiB_2 powders, balance 60A powders and some GCr15 steel balls, were placed into steel jars to mill for 10 h at 450 rpm to break the powders. Secondly, 2.5 vol. % CNTs and pure ethyl alcohol were added in the above Fe- TiB_2 mixture to further mill at 400 rpm for 5 h. To obtained composite powders with analogously spherical shape and suitable size, spray drying (SD) and plasma spheroidization (PS) treatment were then employed in this work. Finally, the composite feedstocks were deposited on clean grit-blasted 45 steel plates with dimensions of 60 mm \times 40mm \times 5 mm. The optimized spraying parameters were listed in Table 1. In addition, Fe- TiB_2 cermet coating without CNT addition prepared with above same process, and sole sprayed Fe-based metallic coating were prepared for comparison purpose.

Table 1 Spraying parameters used in the HVOF process.

Parameters	Values
Torch velocity (mm/s)	400
Spraying distance (mm)	180
Powder feed rate (%)	20
Fuel gas pressure (psi)	97/102
Compressed air pressure (psi)	107
Carrier gas pressure (L/min)	68
Number of passes	10
Step size (mm)	5
Air to fuel ratio	1.1

2.2 Characterizations

The morphologies of powders and coatings were observed via field emission scanning electron microscopy (Nova Nano 430). The detailed microstructure of the (Fe- TiB_2)/CNT composite coating was study with the high resolution transmission electron microscopy (TEM, JEM-3200FS). X-ray diffraction (XRD) analyses of powders were determined on a Philips X-Pert Pro diffractometer with Cu-K_α radiation source. The particle size distribution (PSD) was measured by laser diffraction system (Better size 2000LD) with a wet dispersion technique. Image analyzing method was employed to measure the porosity of the coatings. Microhardness and fracture toughness tests were performed using a Digital Microhardness Tester on the polished cross sections of coatings under a load of 2.94 N

and 49 N for 15 s dwell time, respectively. The fracture toughness of coatings were measured by the Evans and Wilshaw equation [16].

2.3 Wear testing

As for the wear test, all samples with dimensions of 15 mm × 15 mm × 5 mm were polished and carried out via the SFT-2M type pin-on-disk friction tester at room temperature. Φ4 mm Si₃N₄ balls were used as the wear counter-face. The test parameters were as follows: 3 mm for radius of rotation, 16 N and 32 N for applied load, 180 m for total sliding distance, and a fixed sliding time of 30 min. Three repeats were done for the wear test on each coating to make the data reliable. Combined with the profiles of wear scars, the specific wear rate was calculated by:

$$K = \frac{2\pi r \cdot S}{N \cdot D} \quad (1)$$

Where K is the specific wear rate (mm³ / N·m); V is the volume loss (mm³) which equal to 2πr·S; r is the radius of rotation (mm); and S is the area by integrating the curvilinear function of profiles (mm²); N is the applied load (N); and D is the total sliding distance (m).

2.4 Electrochemical measurement

The corrosion properties of the coatings were evaluated by using a Potentiostat/Galvanostat (PGSTAT302N) with standard saturated calomel electrode and platinum auxiliary electrode. The working electrode was exposed to a circular area with diameter of 10 mm. 3.5 wt. % NaCl aqueous solutions were used as electrolyte. First, the clean and polished samples were immersed in the solution for 60 min until the open circuit potential became steady. Potentiodynamic polarization curves were measured with a potential sweep rate of 0.1 mV/s from -0.1 V to 1 V.

3. Results and discussion

3.1 Morphology of the SD powders

Fig. 1 shows the surface morphologies of the powders after spray drying. It is observed from Fig. 1a that most SD powders achieved a favorable shape and size ranged from about 15 to 50 μm. However, quite a few pores were also found in each powder. Fig. 1b presents the magnified view of one typical SD powder, revealing that the powder was mainly consisted of broken 60A particles and undeformed TiB₂ powders. It is noted that the distribution of CNT (marked in white arrows) was homogeneous. Thus, after SD process, nearly spherical but relatively loose composite powders with favorable distribution of TiB₂ particles and CNTs were acquired.

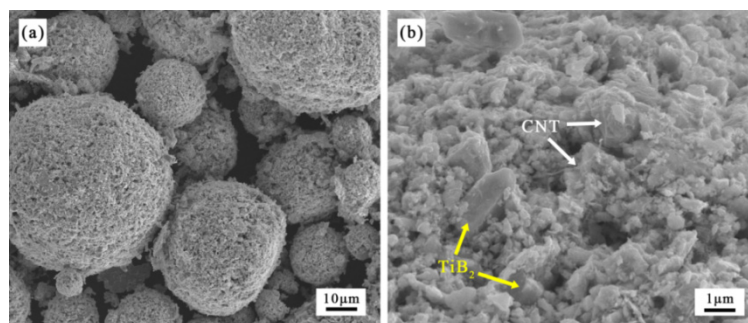


Fig. 1. Morphology of the SD powders: (a) A whole view; and (b) Shows the distribution of the CNTs and TiB₂ powders.

3.2 Morphology of the PS powders

Fig. 2 shows the characterized results of the PS powders. Among them, Fig. 2a exhibits that the powders have mostly achieved a spherical shape, and the pristine pores were disappeared. In addition,

seen from the backscattered electron image of Fig. 2b, it is found that the powder interior was also dense, and the TiB_2 powders were uniformly wrapped into the PS powder. The PS treatment is known as an effective approach to densify powders via partly or fully remelting and spherify them with surface tension. Due to the holding time of powders during PS process is very short, thus the good distribution state of TiB_2 and CNTs can remain from the SD powders to the PS powders. The XRD pattern of the PS powders was depicted as Fig. 2c. It is indicated that their main phases was austenite, ferrite and TiB_2 phase. Lastly, Fig. 2d further confirmed that the PSD of PS powders are +6-43 μm , suggesting a favorable spraying size.

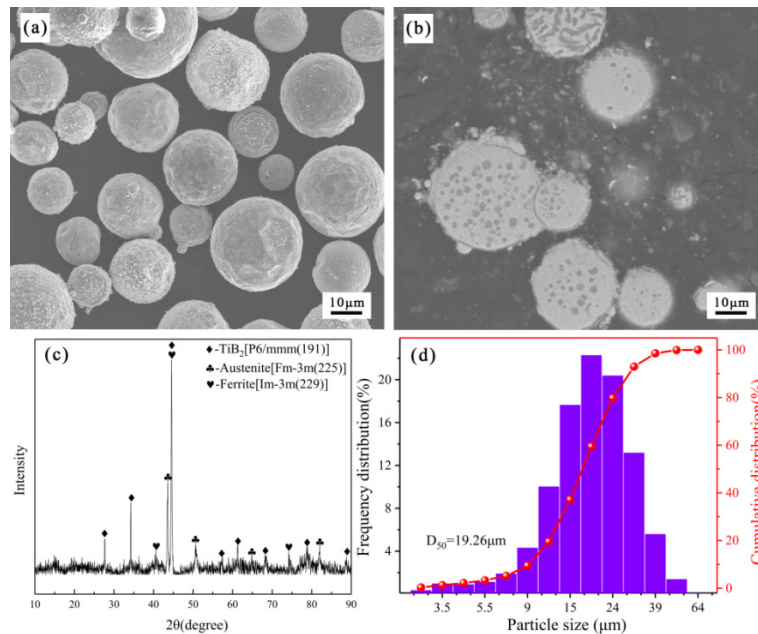


Fig. 2. Characterized results of the PS powders: (a) A whole view; (b) Cross-sectional microstructure; (c) XRD pattern; and (d) PSD result.

3.3 Microstructure of the composite coating

Fig. 3 presents the surface and cross-sectional morphologies of the $(\text{Fe-TiB}_2)/\text{CNT}$ composite coating. Observed from Fig. 3a, the coating exhibited “pancake” morphology with few un-melted particles, revealing a favorable melting state after doping TiB_2 and CNTs. Fig. 3b shows that the composite coating possessed thickness over 250 μm , and the TiB_2 powders were uniformly dispersed in the Fe alloy matrix.

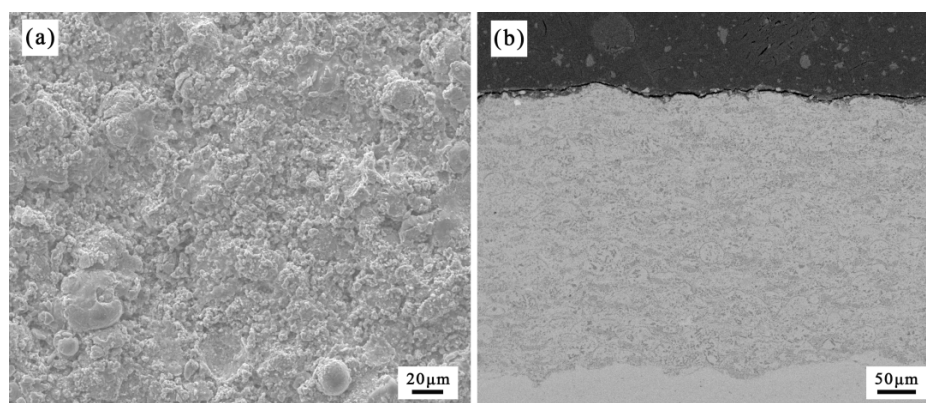


Fig. 3. Morphology of the composite coatings: (a) Surface morphology; and (b) Cross-sectional microstructure.

Fig. 4 shows the bright field TEM image of the (Fe-TiB₂)/CNT composite coating. Fig. 4a exhibits a typical view that TiB₂ phase was dispersed in the Fe alloy matrix. To evaluate the interface between the TiB₂ and Fe alloy, the corresponding region from Fig. 4a was selected to magnify as shown in Fig. 4b. A lattice spaces of 0.32 nm was measured, which agrees well with that of TiB₂ (001) plane. It is worth mentioning that the interface bonding between TiB₂ and Fe alloy was clean and tight. It is well known that the interface bond of different phases was a crucial issue for the composite materials [17, 18]. And, the strong interface strength can greatly reduce the failure at the interfaces, and best exert the synergistic effect of the reinforcements [19].

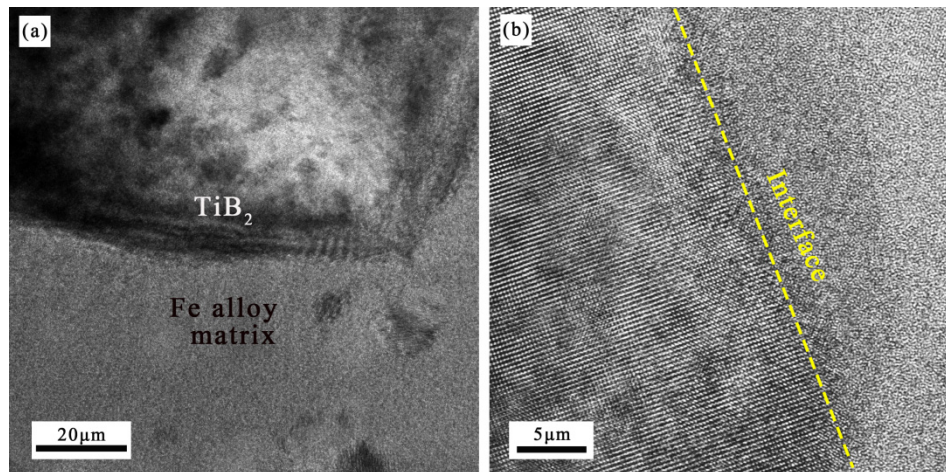


Fig.4. Microstructure of the composite coatings: (a) Bright field TEM image; and (b) Showing the Fe-TiB₂ interface.

To further compare the properties of the three types of coatings, their microhardness, fracture toughness and porosity were listed in Table 2. It is indicated that the porosity was greatly reduced with doped TiB₂, especially further doping CNTs. Generally, the formation of pores was occurred along the inter-splats. Thus, the super high thermal conductivity (about 3000 W/m·K) of CNT can significantly benefit the melted state of (Fe-TiB₂)/CNT composite coating, and then contribute to tight bond between the inter-splats. In term of the hardness of the coatings, both the introduction of large amount of small-sized hard TiB₂ phase (about 34GPa) and the CNTs with super high strength (about 100GPa), especially in a homogenous state, can increase the resistance of coating to the indentation deformation. Similarly, the fracture toughness of the coatings also obtained obvious enhancement. Due to the cracks were commonly initiated at the pores or other fragile regions, the lowest porosity and the well-dispersed CNTs with ultrahigh Young's modulus (~1 TPa) render the (Fe-TiB₂)/CNT composite coating the highest fracture toughness. In addition, implied from the table 2, both doped TiB₂ or CNTs, the coating roughness was improved.

Table 2 Properties of the coatings prepared by HVOF.

Coating type	Porosity (%)	Microhardness (HV _{0.3})	Fracture toughness (MPa·m ^{1/2})	Roughness (μm)
Fe-based metallic	2.80±0.35	368	1.41	3.5±0.4
Fe-TiB ₂ cermet	1.16±0.21	662	3.18	3.0±0.2
(Fe-TiB ₂)/CNT composite	0.71±0.14	874	4.57	2.4±0.1

3.4 Tribological properties

Table 3 respectively displays the coefficient of friction (COF), volume loss and specific wear rate of the coatings. It is found that the (Fe-TiB₂)/CNT composite coating exhibit superior wear resistance for

its lowest wear damage. With increased the wear load to 32 N, the composite coating was more seriously destroyed due to larger wear force.

Table 3 Wear test results of the coatings.

Coating type	Load (N)	COF	Volume loss (10^{-2} mm^3)	Specific wear rate ($10^{-6} \text{ mm}^3 \cdot \text{N}^{-1} \cdot \text{m}^{-1}$)
Fe-based metallic	16	0.72	28.5±4.8	98.96±2.4
Fe-TiB ₂ cermet	16	0.46	2.15±0.6	7.47±0.9
(Fe-TiB ₂)/CNT composite	16	0.67	0.71±0.2	2.47±0.5
(Fe-TiB ₂)/CNT composite	32	0.52	2.29±0.7	7.95±1.1

To reveal the wear mechanism of the (Fe-TiB₂)/CNT composite coating, Fig. 5 presents the backscattered electron image of its worn scars with the wear load at 16 N and 32 N, respectively. The wear groove seen in Fig. 5a was smooth without obvious ploughing and delamination, revealing the abrasive wear is slight. However, it is noted that large-scale oxidation was observed in the wear track. Due to the sequence of oxygen affinity for the elements in this study are $\text{Ti} > \text{Si} > \text{Fe} > \text{Cr} > \text{Ni}$. Thus, the wrapped TiB₂ can be preferentially oxidized where the wear happened. While worn at 32 N, quite a few rugged pits were formed (see Fig. 5b). This is because the oxidative wear was aggravated, and the more delamination further led to increase of the wear volume loss. In general, the wear resistance of the (Fe-TiB₂)/CNT composite coating was favorable, even in the higher wear load. The main wear down mechanisms of the composite coating was mild oxidative and slight abrasive wears.

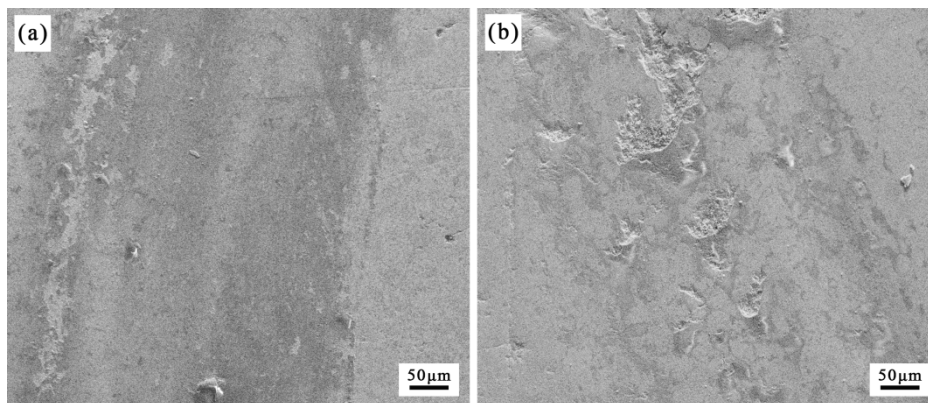


Fig. 5. Morphology of the worn scars of the composite coating: (a) at 16 N; and (b) at 32 N.

3.5 Corrosion properties

The potentiodynamic polarization curves as Fig. 6 were employed to evaluate the corrosion properties of the coatings in NaCl solution. It is indicated that the (Fe-TiB₂)/CNT composite coating exhibits much better corrosion properties than the substrate. With the applied potential increased, the composite coating had a wide passive region with a high potential of pitting initiation. While the substrate nearly had no passive process, implied it was easy to be corroded. The difference in corrosion potential and corrosion current density further implied that the coating doped TiB₂ and CNTs can greatly prevent the substrate from corrosion invasion. Owing to the pores usually be regarded as the diffusion channels for electrolyte to cause inner corrosion. Thus, the better corrosion property of the (Fe-TiB₂)/CNT composite coating is ascribed to the dense microstructure with lowest porosity and the good interface bond of Fe-TiB₂.

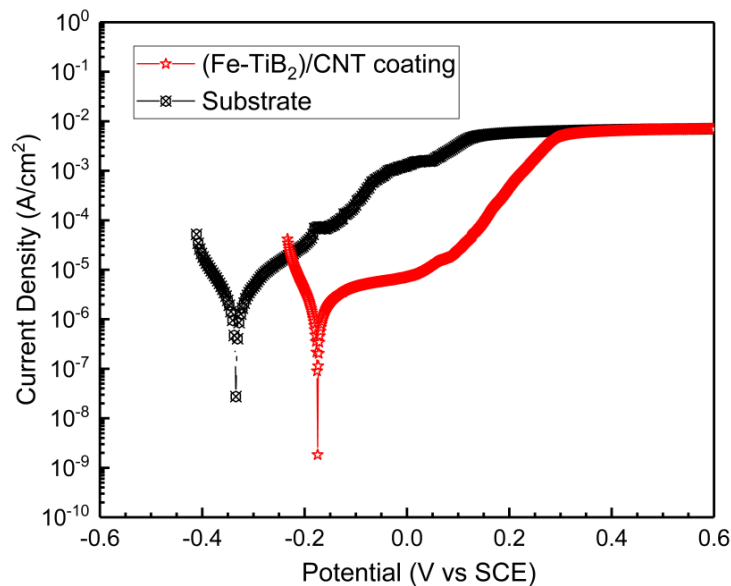


Fig. 6. Potentiodynamic polarization curves of the composite coating and the substrate.

Fig. 7 shows the corrosion morphology of the (Fe-TiB₂)/CNT composite coating after the electrochemical test. It is evident that the pores may be the preferential corrosion sites due to the storage of corrosion media. And, the corrosion was also occurred at the inter-splats and left some etch pores. In addition, owing to the distinguished corrosion potentials of TiB₂ phase and Fe alloy, pitting was occasionally observed in the coating surface. Thus, the main corrosion failure mechanism of (Fe-TiB₂)/CNT composite coating was pitting at the pores and along the inter-splats or Fe-TiB₂ interfaces.

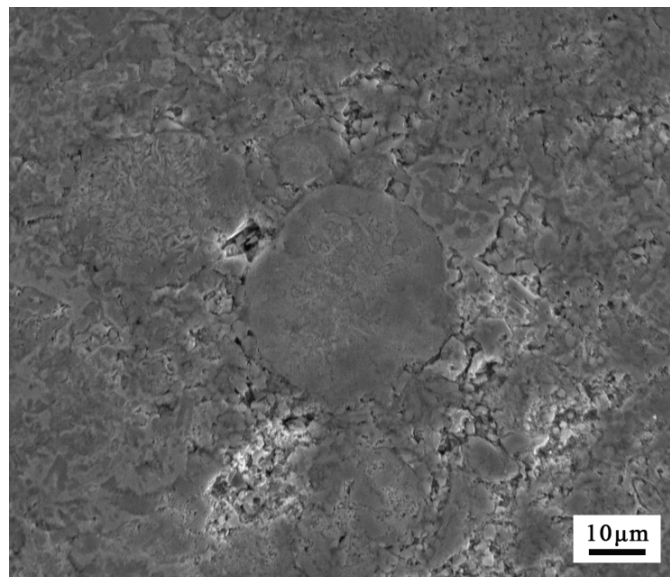


Fig. 7. Morphology of corroded surface about the (Fe-TiB₂)/CNT composite coating after electrochemical test.

4. Conclusions

In this work, (Fe-TiB₂)/CNT composite coating were deposited on mild steel via HVOF technique. And its microstructure evolution of powders, tribological and corrosion behavior were investigated. The main conclusions are as follows.

1. Composite feedstocks with uniform TiB₂ and CNTs were successfully prepared through BM, SD, PS processes.
2. The introduction of the TiB₂, especially the CNTs, can render the coating a lower porosity, favorable microstructure, improved microhardness and fracture toughness.
3. The (Fe-TiB₂)/CNT composite coating obtained superior wear and corrosion resistance.

Acknowledgments

This work was supported by the National Natural Science Foundation of China (Grant No. 51901079), the Fundamental Research Funds for the Central Universities, the Opening Project of National Engineering Research Center for Powder Metallurgy of Titanium & Rare Metals, the Natural Science Foundation of Guangdong Province (No. 2018A030313615, 2018A030310406, 2020A1515010736), the Guangzhou Municipal Science and Technology Program (No. 202007020008), the Zhongshan Municipal Science and Technology Program (Platform Construction and innovation Team) (2016F2FC0005), the Research and industrialization of key technology of high efficiency non-oriented electrical steel (191007102629094) and Zhongshan Collaborative Innovation Fund (2018C1001).

References

- [1] E. Sadeghimeresht, N. Markocsan, P. Nylén, Microstructural characteristics and corrosion behavior of HVAF- and HVOF-sprayed Fe-based coatings, *Surface & Coatings Technology*, 318 (2017) 365-373.
- [2] Bolelli. Giovanni, Colella. Alberto, Lusvarghi. Luca, Puddu. Pietro, Rigon. Rinaldo, Sassatelli. Paolo, T. Veronica, Properties of HVOF-sprayed TiC-FeCrAl coatings, *Wear*, 418-419 (2019) 36-51.
- [3] X. Liu, M. Xiao, M. Liu, Z. Qiu, D. Zeng, Preparation and enhanced wear resistance of HVAF-sprayed Fe-TiB₂ cermet coating reinforced by carbon nanotubes, *Surface and Coatings Technology*, 408 (2021).
- [4] Anil Kumar, Rahul Kumar, Pavan Bijalwan, Monojit Dutta, Atanu Banerjee, T. Laha, Fe-based amorphous/nanocrystalline composite coating by plasma spraying: Effect of heat input on morphology, phase evolution and mechanical properties, *Journal of Alloys and Compounds*, 771 (2019) 827-837.
- [5] P. Bijalwan, A. Kumar, S.K. Nayak, A. Banerjee, M. Dutta, T. Laha, Microstructure and corrosion behavior of Fe-based amorphous composite coatings developed by atmospheric plasma spraying, *Journal of Alloys and Compounds*, 796 (2019) 47-54.
- [6] G.R.Q. Zhang C , Yang Y, Y. Wu, L. Liu, Influence of the size of spraying powders on the microstructure and corrosion resistance of Fe-based amorphous coating, *Electrochimica Acta*, 56 (2011) 6380-6388.
- [7] Zhang Huan, Xie Youtao, Huang Liping, Huang Shansong, Zheng Xuebin, C. Guang, Effect of feedstock particle sizes on wear resistance of plasma sprayed Fe-based amorphous coatings, *Surface and Coatings Technology*, 258 (2014) 495-502.
- [8] R.Q. Guo, C. Zhang, Q. Chen, Y. Yang, N. Li, L. Liu, Study of structure and corrosion resistance of Fe-based amorphous coatings prepared by HVAF and HVOF, *Corrosion Science*, 53 (2011) 2351-2356.
- [9] Z. Chu, F. Wei, X. Zheng, C. Zhang, Y. Yang, Microstructure and properties of TiN/Fe-based amorphous composite coatings fabricated by reactive plasma spraying, *Journal of Alloys and Compounds*, 785 (2019) 206-213.
- [10] C.Z. H. Zhou, W. Wang, M. Yasir, L. Liu, Microstructure and Mechanical Properties of Fe-based Amorphous Composite Coatings Reinforced by Stainless Steel Powders, *Journal of Materials Science & Technology*, 35 (2015) 43-47.
- [11] Z. Chu, X. Zheng, C. Zhang, J. Xu, L. Gao, Study the effect of AT13 addition on the properties of AT13/Fe-based amorphous composite coatings, *Surface and Coatings Technology*, 379 (2019) 125053.

- [12] Y.S. Wu, D.C. Zeng, Z.W. Liu, W.Q. Qiu, X.C. Zhong, H.Y. Yu, S.Z. Li, Microstructure and sliding wear behavior of nanostructured Ni60-TiB₂ composite coating sprayed by HVOF technique, *Surface & Coatings Technology*, 206 (2011) 1102-1108.
- [13] Y. Zou, Y. Wu, G. Zou, G. Wang, Z. Zheng, Z. Qiu, M. Liu, D. Zeng, Tribological properties and corrosion behavior of AC-HVAF sprayed nanostructured NiCrCoAlY-TiB₂ coatings, *Surface and Coatings Technology*, 406 (2021)126739.
- [14] Y.S. Wu, W.Q. Qiu, H.Y. Yu, X.C. Zhong, Z.W. Liu, D.C. Zeng, S.Z. Li, Cycle oxidation behavior of nanostructured Ni60-TiB₂ composite coating sprayed by HVOF technique, *Applied Surface Science*, 257 (2011) 10224-10232.
- [15] P.T. S. Moonngam, D. Deesom, C. Banjongprasert Fe-Cr/CNTs nanocomposite feedstock powders produced by chemical vapor deposition for thermal spray coatings, *Surface & Coatings Technology*, 306 (2016) 323-327.
- [16] A.G. Evans, T.R. Wilshaw, Quasi-static solid particle damage in brittle solids-I. Observations analysis and implications, *Acta Metallurgica*, 24 (1976) 939-956.
- [17] X.Q. Liu, C.J. Li, J.H. Yi, K.G. Prashanth, N. Chawake, J.M. Tao, X. You, Y.C. Liu, J. Eckert, Enhancing the interface bonding in carbon nanotubes reinforced Al matrix composites by the in situ formation of TiAl₃ and TiC, *Journal of Alloys and Compounds*, 765 (2018) 98-105.
- [18] M.S. Baisong Guo, Jianhong Yi, Song Ni, Tao Shen, Yong Du, Improving the mechanical properties of carbon nanotubes reinforced pure aluminum matrix composites by achieving non-equilibrium interface, *Materials and Design*, 120 (2017) 56-65.
- [19] X.Q. Liu, C.J. Li, X. You, Z.Y. Xu, X. Li, R. Bao, J.M. Tao, J.H. Yi, Size-dependent effects of Ti powders in the pure aluminum matrix composites reinforced by carbon nanotubes, *Journal of Alloys and Compounds*, 823 (2020)153824.